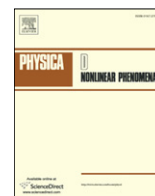




ELSEVIER

Contents lists available at ScienceDirect

Physica D

journal homepage: www.elsevier.com/locate/physd

Periodic solutions of a singularly perturbed delay differential equation

Mohit H. Adhikari^{a,*}, Evangelos A. Coutsias^b, John K. McIver^a

^a Department of Physics and Astronomy, University of New Mexico, Albuquerque, New Mexico, 87131, United Kingdom

^b Department of Mathematics and Statistics, University of New Mexico, Albuquerque, New Mexico, 87131, United Kingdom

ARTICLE INFO

Article history:

Received 31 October 2007

Received in revised form

23 July 2008

Accepted 26 July 2008

Available online xxxx

Communicated by R. Roy

PACS:

02.30.Ks

02.70.Hm

45.10.Hj

Keywords:

Singularly perturbed delay-differential equation

Hopf bifurcation

Slowly oscillating periodic solutions

Chebyshev polynomials

Iterated maps

ABSTRACT

A singularly perturbed differential delay equation of the form

$$\epsilon \dot{x}(t) = -x(t) + f(x(t-1), \lambda) \quad (1)$$

exhibits slowly oscillating periodic solutions (SOPS) near the first period-doubling bifurcation point of the underlying map (obtained by setting $\epsilon = 0$). For extremely small values of ϵ , these periodic solutions resemble square waves, which consist of sharp, $O(\epsilon)$ transition layers connecting intervals of approximately unit length. In this article, we obtain analytic expressions for these square-wave periodic solutions, by solving the corresponding transition layer equations, and show that they are in excellent agreement with numerical solutions for a range of values of ϵ and λ . We also derive analytic expressions for other periodic solutions which are odd harmonics of the SOPS, and numerically exhibit their instability near the first period doubling bifurcation point of the map. The numerical computations were performed using a high accuracy Chebyshev spectral scheme. We give a brief description together with a study of its accuracy and efficiency.

© 2008 Elsevier B.V. All rights reserved.

1. Introduction

In recent years, a singularly perturbed delay differential equation of the form

$$\epsilon \dot{x}(t) = -x(t) + f(x(t-1), \lambda) \quad (2)$$

has served as a model for physiological control systems [22] and for the transmission of light through a ring cavity [15, 19, 17]. Here \dot{x} denotes the derivative of x , with respect to the dimensionless time t ($t \equiv t'/r$, where r is the delay time). $\epsilon \equiv \tau/r > 0$ is a small parameter defined as the ratio of the linear decay time (τ) of the dependent variable to the delay and $f(x, \lambda)$ represents a nonlinear function of x with λ being a control parameter. Setting ϵ to 0 reduces Eq. (2) to a map:

$$x_n = f(x_{n-1}, \lambda) \quad (3)$$

whose dynamical properties are expected to reflect themselves in the solution of the differential equation, when ϵ is small. Significant contributions to understanding the relationship between the behavior of the map, and that of the flow of the differential equation (2) have been made by Chow and Mallet-Paret [7], Mallet-Paret and Nussbaum [24], Chow et al. [6] and Hale and Huang [14, 13]. Mallet-Paret and Nussbaum [23, 24] have shown that if the fixed point, $x_0 = f(x_0, \lambda)$, of the map loses its stability through a period-doubling bifurcation as λ crosses a critical value λ_0 then, under certain conditions on $f(x, \lambda)$, there exists an $\epsilon_0(\lambda) > 0$ such that for $0 < \epsilon < \epsilon_0$, there is a slowly oscillating periodic solution (SOPS) to the differential equation (2) of period close to, but greater than, 2. A SOPS is a periodic solution, such that the interval between its successive zeroes (i.e. successive crossings with x_0) is greater than 1. As ϵ decreases from ϵ_0 to 0 for a given λ close to λ_0 , these solutions change their shape from sinusoidal to square-waves. The square-wave SOPS consist of sharp transition layers of order ϵ connecting flat plateaus of order 1 that are close to the period-2 fixed points of the map.

* Corresponding author. Tel.: +44 117 331 7374.

E-mail address: Mohit.Adhikari@bristol.ac.uk (M.H. Adhikari).

Now, in the neighborhood of the fixed point x_0 , one can expand a generic nonlinear function $f(x_0, \lambda)$ in a Taylor series about x_0 . Let $x(t) = x_0(\lambda) + y(t)$, then Eq. (2) becomes,

$$\epsilon \dot{y}(t) + y(t) = a_1 y(t-1) + a_2 y^2(t-1) + a_3 y^3(t-1) + \dots \quad (4)$$

where $a_1 = f'(x_0, \lambda)$, $a_2 = f''(x_0, \lambda)$ and so on. Thus the fixed point is shifted to 0, and the series can be truncated so that $f(x, \lambda)$ in (2) can be replaced by the first few nonlinear terms in the corresponding Taylor series. Chow et al. [6] make the specific assumption that

$$\begin{aligned} f(x, \lambda) &= -f(-x, \lambda) \\ &= -(1 + \lambda)x + x^3 + o(x^3) \quad \text{as } x \rightarrow 0 \end{aligned} \quad (5)$$

where for $\epsilon = 0$, the point $\lambda = 0$ corresponds to a period-doubling bifurcation point for the map. They then show that the SOPS of (2) are in one-to-one correspondence with the periodic solutions of a particular perturbed, planar Hamiltonian system, obtained by an application of the theory of center manifolds. Further, they show that in the limit $(\lambda, \epsilon) \rightarrow 0$, the period of the square-wave solutions can be expressed as $2 + 2\epsilon + o(|\epsilon|(|\lambda| + |\epsilon|))$.

Chow and Mallet-Paret [7] obtain a similar result for the period of square-wave SOPS in the case of a cubic nonlinearity as in (5), by a different approach than Chow et al. [6]. They formulate a set of coupled delay-differential equations modeling the sharp transition layers, and solve them using a two parameter perturbation expansion. The resulting leading order ordinary differential equation is exactly the unperturbed Hamiltonian equation obtained by Chow et al. [6].

More recently, Erneux et al. [10] used a modified Poincaré–Lindstedt method to solve the original delay-differential equation (2) with a generic non-linearity, in both small as well as large delay limits, near the first period-doubling bifurcation. They compare the analytical and numerical bifurcation diagrams as the oscillations progressively change from sine-to-square waves.

In this paper, we consider the following equation,

$$\epsilon \dot{x}(t) = -x(t) + \lambda x(t-1)(1 - x(t-1)). \quad (6)$$

Logistic nonlinearity is chosen, because we are interested in studying the periodic solutions of (2) in the neighborhood of x_0 . In this region, as shown in (4), any generic nonlinear function $f(x, \lambda)$ can be approximated by a quadratic nonlinearity. One can then scale $x(t)$ appropriately, so that the corresponding equation reduces to (6) to leading order. Since the logistic map undergoes its first period-doubling bifurcation at $\lambda = 3$, it can be shown that it satisfies the conditions for the existence of slowly oscillating periodic solutions of (6) in the neighborhood of $\lambda = 3$.

The square-wave SOPS of (6) near $\lambda = 3$ exhibit a peculiar asymmetry. If one measures the time intervals between three successive crossings of the square-wave solution with the average of the period-2 fixed points of the map, one of them turns out to be $\sim 1 + 2\epsilon$, while the other is $O(1)$. Taking note of this observation, we formulate the corresponding transition layer equations and solve them using an approach similar to the one used by Chow and Mallet-Paret [7]. By employing a two-parameter perturbation expansion in ϵ and $\sigma = \sqrt{\lambda - 3}$ for the two “half-periods”, and using an appropriate scaling between ϵ and σ , we obtain analytic expressions for the square-wave SOPS in the neighborhood of the first period-doubling bifurcation point of the map. The leading order equation again represents the unperturbed Hamiltonian system obtained by Chow et al. [6] and Hale and Huang [13], however, it does not explain the observed asymmetry in the solution. We calculate the next order correction, which not only explains this asymmetry, but also gives a much better agreement between the overall analytic expression and the form of the solutions obtained by integrating (6) numerically. An accurate expression for the period of these solutions, as a function of ϵ and λ is also obtained.

Further, we use our approach to obtain analytic expressions for other periodic solutions of (6) which can be considered as odd harmonics of the SOPS. By using the leading order approximations for these solutions as initial functions over the interval $[-1, 0]$, we integrate (6) numerically to show that, in the neighborhood of the first period-doubling bifurcation point of the map, these initial functions are eventually attracted to the SOPS and not to the odd harmonic periodic solutions.

Our derivation of the asymptotic expressions for the square-wave SOPS is not limited to the specific logistic nonlinear functional form used in Eq. (6). It can be generalized to any generic nonlinearity as sketched in Appendix A.

Numerical integration of (6) is done using an efficient spectral algorithm based on a method devised by Coutsias et al. [9,8] to integrate ordinary differential equations with rational function coefficients. The algorithm is outlined in Appendix B, and its accuracy in obtaining periodic solutions of linear scalar delay-differential equations as well as the square-wave solutions of (6) is compared with that of RADAR5 [12], a state-of-the-art Runge–Kutta method.

The paper is organized as follows: In Section 2, we re-derive the Hopf bifurcation curve relating λ and ϵ and the transition layer equations. The main result of this paper is presented in Section 3, in which we derive analytic expressions for the square-wave SOPS in terms of elliptic functions using a perturbation analysis, and show the agreement between the analytical and the numerical results for different values of λ and ϵ . Section 4 deals with the odd-harmonic solutions and their stability, and we discuss our results and, in particular, compare the scaling used by us with the one used by Erneux et al. [10] in the final section.

2. Background

2.1. Fixed points of the logistic map

The logistic map is given by

$$x_n = \lambda x_{n-1}(1 - x_{n-1}). \quad (7)$$

It has two fixed points at 0 and at $x_0(\lambda) = 1 - \frac{1}{\lambda}$. For $0 < \lambda < 1$, only the trivial fixed point is stable. For $1 \leq \lambda < 3$, the trivial fixed point is unstable and only $x_0(\lambda)$ is stable. At $\lambda = 3$, x_0 becomes unstable and goes through a period-doubling bifurcation giving rise to two period-2 fixed points x_+ and x_- given by

$$x_{\pm} = a \pm b; \quad a = \frac{\lambda + 1}{2\lambda}; \quad b = \frac{\sqrt{(\lambda + 1)(\lambda - 3)}}{2\lambda}. \quad (8)$$

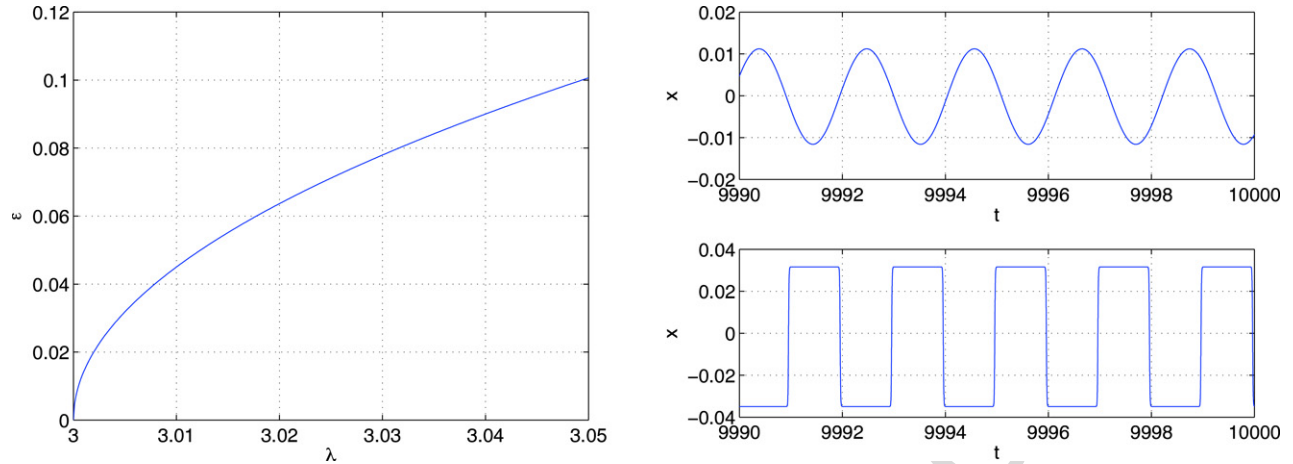


Fig. 1. Left: The Hopf bifurcation curve. Right (top): The sinusoidal solution ($\lambda = 3.01$ and $\epsilon \approx 0.045$). Right (bottom): The square-wave solution ($\lambda = 3.01$ and $\epsilon = 0.01$).

Thus if Eq. (7) is written as

$$x(t) = \lambda x(t-1)(1-x(t-1)) \quad (9)$$

then as λ crosses the value 3, the steady state solution $x(t) = x_0$ loses stability to a periodic solution of period 2. This periodic solution becomes unstable at $\lambda \approx 3.45$ and bifurcates into a period-4 solution which, as λ increases further, bifurcates into a period-8 solution and so on, thus following a period-doubling route to chaos.

2.2. The Hopf bifurcation curve

As the logistic map undergoes its first period-doubling bifurcation, the solution to the delay equation (6) also exhibits a Hopf bifurcation from a stationary state $x(t) = x_0$ to a SOPS of period approximately equal to 2. However, the value of λ at which this bifurcation occurs depends on the value of ϵ . Chow and Mallet-Paret [7] show that the constant solution $x(t) = x_0$ loses its stability along a curve in the $\lambda - \epsilon$ plane. This section derives an expression for this curve relating λ and ϵ in the limit $(\lambda, \epsilon) \rightarrow (3, 0)$ [3,26].

Linearizing equation (6) about the fixed point x_0 of the map gives,

$$\epsilon \dot{\eta}(t) + \eta(t) - \alpha \eta(t-1) = 0 \quad (10)$$

where $x(t) = x_0 + \eta(t)$ and $\alpha \equiv \alpha(\lambda) = \lambda(1-2x_0) = 2 - \lambda$. The characteristic equation of Eq. (10), obtained by substituting $\eta(t) = e^{st}$, has exactly two roots with zero real part while other roots have negative real parts when ϵ, α satisfy the equations

$$\tan(\omega_0) = -\epsilon \omega_0; \quad \epsilon^2 \omega_0^2 = \alpha^2 - 1 \quad (11)$$

where $0 < \omega_0 < \pi$ is the frequency of the SOPS. In the asymptotic limit, as $\epsilon \rightarrow 0$, $\omega_0 \rightarrow \pi$ which corresponds to the period-2 solution of the map.

Let $\sigma = \sqrt{\lambda - 3}$, then α in Eq. (11) can be written as $\alpha = -(1 + \sigma^2)$. Hence the second of Eq. (11) becomes,

$$\epsilon_0^2 \omega_0^2 = 2\sigma^2 + \sigma^4. \quad (12)$$

Close to $\lambda = 3$, the bifurcation point of the map, σ is small and hence $\omega_0 \approx \pi$. One can then ignore $O(\sigma^4)$ term in the above equation and write

$$\epsilon_0 \approx \frac{\sqrt{2}}{\pi} \sigma = \frac{\sqrt{2}}{\pi} \sqrt{\lambda - 3}. \quad (13)$$

Thus for a given $\lambda > 3$, there exists an ϵ_0 , such that for $0 < \epsilon < \epsilon_0$, there exist SOPS to Eq. (6). Conversely, for a given $\epsilon > 0$ (delay), such solutions exist, only above a certain value of λ given by (13). Eq. (13) is plotted in the left side of Fig. 1. In the limit, $(\lambda, \epsilon) \rightarrow (3, 0)$, the constant solution $x(t) = x_0$ loses its stability along this Hopf bifurcation curve, giving rise to an asymptotically stable SOPS, when (λ, ϵ) take values to the right of this curve, as shown by Chow and Mallet-Paret [7]. The shape of the SOPS is sinusoidal near this curve i.e. when $\epsilon = O(\sigma)$, however, as shown in the right side of Fig. 1, it resembles a square-wave when $\epsilon = O(\sigma^2)$ or smaller. Here, $x(t)$ is scaled linearly so that $x_0 = 0$. An important thing to note is the marked difference in the amplitudes of the two solutions for the same value of λ , clearly indicating its dependence on the value of ϵ .

2.3. The transition layer equations

A typical asymptotic form of a square-wave SOPS is shown in Fig. 2. If, for any integer n , t_{2n} and t_{2n+1} denote the time instants when the solution crosses a , the average of two period-2 fixed points x_+ and x_- , with negative and positive slopes respectively, then we define the two ‘‘half-periods’’, $1 + \delta_1$ and $1 + \delta_2$ as:

$$t_{2n} - t_{2n-1} = 1 + \delta_1 \quad \text{and} \quad t_{2n+1} - t_{2n} = 1 + \delta_2. \quad (14)$$

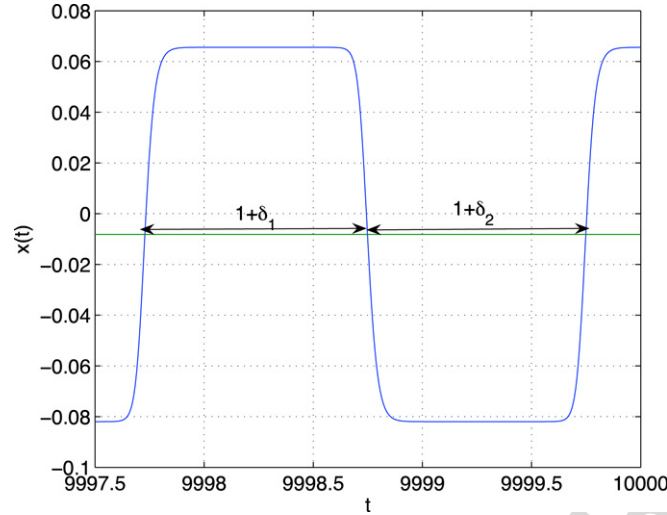


Fig. 2. Asymptotic form of a square-wave solution with definitions of two “half-periods”, $1 + \delta_1$ and $1 + \delta_2$. Here $x(t)$ is scaled so that $x_0 = 0$ and a , the average of x_- and x_+ is negative (The horizontal line in center).

Thus the period of the waveform in Fig. 2 is given by $2 + \delta_1 + \delta_2$. Now one can define

$$U(t) = x(t); \quad V(t) = x(t - 1 - \delta_1). \quad (15)$$

Then the periodicity of the waveform implies,

$$U(t) = V(t - 1 - \delta_2) = V(t + 1 + \delta_1); \quad U(t - 1) = V(t + \delta_1) \quad (16)$$

$$V(t) = U(t - 1 - \delta_1) = U(t + 1 + \delta_2); \quad V(t - 1) = U(t + \delta_2). \quad (17)$$

Substituting in (6) gives,

$$\epsilon U'(t) + U(t) = f(\lambda, V(t + \delta_1)) \quad (18)$$

$$\epsilon V'(t) + V(t) = f(\lambda, U(t + \delta_2)) \quad (19)$$

where, again, $f(x, \lambda) = \lambda x(1 - x)$. In the asymptotic limit $\epsilon \rightarrow 0$, these equations, describe the transition layers that connect the almost flat regions of the square-wave solution [7].

3. Analytic expressions for slowly oscillating periodic solutions

We now solve the transition layer equations using a Poincaré–Lindstedt method in a similar fashion, as done by Chow and Mallet-Paret [7], except, instead of taking an asymptotic limit $\epsilon \rightarrow 0$, we demand periodic solutions to the equations [3]. First, δ_1 and δ_2 are assumed to have the following expansions in terms of (ϵ, σ) :

$$\delta_1 = \epsilon(a_{10} + a_{11}\sigma + a_{12}\sigma^2 + \dots) + \epsilon^2(a_{20} + a_{21}\sigma + a_{22}\sigma^2 + \dots) + O(\epsilon^3)$$

$$\delta_2 = \epsilon(b_{10} + b_{11}\sigma + b_{12}\sigma^2 + \dots) + \epsilon^2(b_{20} + b_{21}\sigma + b_{22}\sigma^2 + \dots) + O(\epsilon^3).$$

Thus the expression for the period of the solution becomes:

$$T = 2 + \delta_1 + \delta_2 \\ = 2 + \epsilon(c_{10} + c_{11}\sigma + c_{12}\sigma^2) + \epsilon^2(c_{20} + c_{21}\sigma) + \epsilon^3(c_{30}) + O(\epsilon\sigma^3, \epsilon^2\sigma^2, \epsilon^3\sigma)$$

where, $c_{ij} = a_{ij} + b_{ij}$. Since the periodic solution to the original Eq. (6) is referenced from the value a , it makes sense to write the transition layer equations in terms of $u(t)$ and $v(t)$ which are defined as:

$$U(t) = a - bu(t); \quad V(t) = a + bv(t). \quad (20)$$

Then the transition layer equations take the form:

$$\epsilon u'(t) + u(t) = v(t + \delta_1) + \mu(v^2(t + \delta_1) - 1) \quad (21)$$

$$\epsilon v'(t) + v(t) = u(t + \delta_2) - \mu(u^2(t + \delta_2) - 1) \quad (22)$$

where, $\mu = \lambda b$:

$$\mu = \frac{\sqrt{(\lambda + 1)(\lambda - 3)}}{2} = \sigma + \frac{\sigma^3}{8} - \frac{\sigma^5}{128} + O(\sigma^7). \quad (23)$$

Next, the time variable is transformed to $s = \frac{\sigma t}{\epsilon}$, so that the period of the solution in terms of s is σ/ϵ . This changes the transition layer equations to

$$\sigma u'(s) + Tu(s) = Tv(s + \xi_1) + T\mu(v^2(s + \xi_1) - 1) \quad (24)$$

$$\sigma v'(s) + Tv(s) = Tu(s + \xi_2) - T\mu(u^2(s + \xi_2) - 1) \quad (25)$$

where $\xi_1 = (\sigma \delta_1)/(\epsilon T)$ and $\xi_2 = (\sigma \delta_2)/(\epsilon T)$. Now $u(s)$ and $v(s)$ are expanded in terms of σ :

$$\begin{aligned} u(s) &= u_0(s) + \sigma u_1(s) + \sigma^2 u_2(s) + \sigma^3 u_3(s) + O(\sigma^4) \\ v(s) &= v_0(s) + \sigma v_1(s) + \sigma^2 v_2(s) + \sigma^3 v_3(s) + O(\sigma^4). \end{aligned}$$

As shown in Eq. (13) in the last section, these SOPS exist for $\epsilon \approx (\sqrt{2}/\pi)\sigma$ or smaller. Further, we are primarily interested in obtaining a functional form of the square-wave solutions, which exist away from the Hopf-bifurcation curve. Hence we choose $\epsilon \sim O(\sigma^2)$ as the distinguished limit and match orders of σ by substituting the expansions given above, in the transition layer equation (24) and (25). It turns out that in the parameter region where these SOPS are sinusoidal in shape, there is a good agreement between the numerical and analytic solutions obtained by using the scaling mentioned above.

To $O(1)$:

$$2u_0(s) = 2v_0(s); \quad 2v_0(s) = 2u_0(s) \quad (26)$$

$O(\sigma)$:

$$\begin{aligned} u'_0 + 2u_1 &= 2v_1 + a_{10}v'_0 + 2v_0^2 - 2 \\ v'_0 + 2v_1 &= 2u_1 + b_{10}u'_0 - 2u_0^2 + 2 \end{aligned}$$

$O(\sigma^2)$:

$$\begin{aligned} u'_1 + 2u_2 + c_{10}u_0 &= 2v_2 + a_{11}v'_0 + a_{10}v'_1 + a_{10}^2 v_0''/4 + 4v_0v_1 + 2a_{10}v_0v'_0 + c_{10}v_0 \\ v'_1 + 2v_2 + c_{10}v_0 &= 2u_2 + b_{11}u'_0 + b_{10}u'_1 + b_{10}^2 u_0''/4 - 4u_0u_1 - 2b_{10}u_0u'_0 + c_{10}u_0 \end{aligned}$$

$O(\sigma^3)$:

$$\begin{aligned} u'_2 + 2u_3 + c_{10}u_1 + c_{11}u_0 &= 2v_3 + (a_{12} + a_{20})v'_0 + a_{11}v'_1 + a_{10}v'_2 + c_{11}v_0 + c_{10}v_1 \\ &\quad + (a_{10}^2 v_1'' + 2a_{10}a_{11}v_0'')/4 + a_{10}^3 v_0'''/24 + 2v_1^2 + 2a_{10}v_1v'_0 + a_{10}^2 v_0'^2/2 \\ &\quad + 4v_0v_2 + 2a_{11}v_0v'_0 + 2a_{10}v_0v'_1 + a_{10}^2 v_0v_0''/2 + (v_0^2 - 1)/4 + c_{10}(v_0^2 - 1) \\ v'_2 + 2v_3 + c_{10}v_1 + c_{11}v_0 &= 2u_3 + (b_{12} + b_{20})u'_0 + b_{11}u'_1 + b_{10}u'_2 + c_{11}u_0 + c_{10}u_1 \\ &\quad + (b_{10}^2 u_1'' + 2b_{10}b_{11}u_0'')/4 + b_{10}^3 u_0'''/24 - 2u_1^2 - 2b_{10}u_1u'_0 - b_{10}^2 u_0'^2/2 \\ &\quad - 4u_0u_2 - 2b_{11}u_0u'_0 - 2b_{10}u_0u'_1 - b_{10}^2 u_0u_0''/2 - (u_0^2 - 1)/4 - c_{10}(u_0^2 - 1) \end{aligned}$$

$O(1)$ equations just imply $u_0(s) = v_0(s)$. Using this in the $O(\sigma)$ equations gives

$$a_{10} + b_{10} = c_{10} = 2 \quad (27)$$

$$u_1(s) - v_1(s) = \left(\frac{a_{10} - b_{10}}{4} \right) u_0'(s) + u_0^2(s) - 1. \quad (28)$$

Adding the $O(\sigma^2)$ equations gives the equation for $u_0(s)$:

$$u_0'' + 2c_{11}u_0' + 2c_{10}^2(u_0 - u_0^3) = 0. \quad (29)$$

Since $u_0(s)$ has to be a periodic function, $c_{11} = (a_{11} + b_{11})$ must be set to 0. The integral curves of this equation are given by

$$u_0'^2 + 2c_{10}^2 u_0^2 - c_{10}^2 u_0^4 = 2C. \quad (30)$$

In the singular limit, i.e. $\epsilon \rightarrow 0$, it can be easily shown that $u_0(s) \sim \tanh(s)$ with $C \rightarrow 2$ since the boundary conditions in such a limit are: $u_0(s) \rightarrow \pm 1$ as $s \rightarrow \pm\infty$. This is done in [7]. In contrast, we seek a periodic solution in the distinguished limit of $\epsilon \sim O(\sigma^2)$. Hence C is set to $c_{10}^2(1 - \eta^2)/2$, where, $0 < \eta < 1$ can be found from the period of the solution. Eq. (30) implies,

$$s = \int_0^{u_0} \frac{dy}{c_{10} \sqrt{(y^2 - u_{0+}^2)(y^2 - u_{0-}^2)}}$$

where, $u_{0+}^2 = 1 + \eta$ and $u_{0-}^2 = 1 - \eta$ are the roots of the equation, $u_0^4 - 2u_0^2 + (2C/c_{10}^2) = 0$. Thus,

$$c_{10}s = \frac{1}{u_{0+}} \int_0^\phi \frac{d\theta}{\sqrt{1 - k^2 \sin^2 \theta}} \quad (31)$$

where $\sin \phi = u_0/u_{0-}$ and k is the modulus of the elliptic integral of the first kind. k and the complementary modulus k' are given by:

$$k^2 = \frac{1 - \eta}{1 + \eta}; \quad k'^2 = 1 - k^2 = \frac{2\eta}{1 + \eta}. \quad (32)$$

Hence $u_0(s) = v_0(s)$ can be written as

$$u_0(s) = u_{0-} \operatorname{sn}(c_{10}u_{0+}s, k) = \sqrt{1 - \eta} \operatorname{sn} \left(2(\sqrt{1 + \eta})s, k \right). \quad (33)$$

Here $\operatorname{sn}(z, k)$; $z = 2(\sqrt{1 + \eta})s$, is the Jacobi elliptic function.

3.1. Calculation of η

Now, the period of $u_0(s)$ is σ/ϵ . Hence the quarter period $K(k)$ (the complete elliptic integral of the first kind) of $sn(z, k)$ is $(\sigma/2\epsilon)\sqrt{1+\eta}$. But K is also a function of k , the modulus of the elliptic function, which depends on η . Thus given σ and ϵ , η and hence the value of C in Eq. (30) can be calculated by solving the following equation numerically:

$$\frac{1}{2}\sqrt{1+\eta}\frac{\sigma}{\epsilon} = K(k); \quad k^2 = \frac{1-\eta}{1+\eta}. \quad (34)$$

For a given value of σ , as $\epsilon \rightarrow 0$, $\eta \rightarrow 0$ and $k \rightarrow 1$, and the solutions become more square-wave like. In this case, there is an asymptotic expression for $K(k)$ [2,5]:

$$\lim_{k \rightarrow 1} K = \ln(4/k') \quad (35)$$

which implies,

$$\eta = \frac{8 \exp(-2K)}{1 - 8 \exp(-2K)} = \frac{8 \exp(-\sqrt{1+\eta}\sigma/\epsilon)}{1 - 8 \exp(-\sqrt{1+\eta}\sigma/\epsilon)}. \quad (36)$$

3.2. The first order corrections

The equations for $u_1(s)$ and $v_1(s)$ turn out to be:

$$u_1'' + 8(1 - 3u_0^2)u_1 = -2(4/3 + \gamma_2)u_0' + 8u_0^2u_0' - 4\eta^2 \quad (37)$$

$$v_1'' + 8(1 - 3u_0^2)v_1 = -2(4/3 + \gamma_2)u_0' + 8u_0^2u_0' + 4\eta^2. \quad (38)$$

Here, $\gamma_2 = c_{12} + c_{20}$. $u_0'(s) = v_0'(s)$ is clearly a solution to the homogenous part of each of these two equations.

First, we try to find the value for γ_2 . The solvability condition for Eq. (37) requires,

$$-2(4/3 + \gamma_2) \int_0^{\sigma/\epsilon} u_0'^2(s) ds + 8 \int_0^{\sigma/\epsilon} u_0^2(s)u_0'(s) ds - 4\eta^2 \int_0^{\sigma/\epsilon} u_0'(s) ds = 0. \quad (39)$$

Let $\Gamma = -(4/3 + \gamma_2)$. Then Eq. (39) implies,

$$\Gamma \int_0^{4K} cn^2(z)dn^2(z)dz + (1-\eta) \int_0^{4K} sn^2(z)cn^2(z)dn^2(z)dz = 0. \quad (40)$$

These integrals can be done analytically [5] yielding,

$$\gamma_2 = c_{12} + c_{20} = -\frac{8}{15} - \frac{12}{5}\eta^2 \frac{(K(k) - E(k))}{(E(k) - \eta K(k))}. \quad (41)$$

Here, $E(k)$ is the complete elliptic integral of the second kind given by,

$$E(k) = \int_0^K (dn^2(u))du = \int_0^{\pi/2} \sqrt{1 - k^2 \sin^2 \theta} d\theta. \quad (42)$$

Thus, given σ and ϵ , the values of η , k , $K(k)$ and $E(k)$ and hence γ_2 and a more accurate value for the period of these solutions can be found. Numerical evidence suggests that $c_{20} \approx 0$ (a_{20} and b_{20} individually are not zero). Thus the expression for the period becomes,

$$T = 2 + \epsilon(2 + c_{12}\sigma^2 + O(\sigma^3)); \quad c_{12} = -\frac{8}{15} - \frac{12}{5}\eta^2 \frac{(K(k) - E(k))}{(E(k) - \eta K(k))}. \quad (43)$$

In the limit $\epsilon \rightarrow 0$, since $\eta \sim \exp(-2K)$ and $K \gg E$, it is clear from (41) that $c_{12} \approx -8/15$. Hence, an analytic expression for the period of the square-wave SOPS can be written as:

$$T \approx 2 + 2\epsilon \left(1 - \frac{4}{15}\sigma^2 + O(\sigma^3) \right). \quad (44)$$

This is exactly the expression that Chow and Mallet-Paret [7] have derived for the period of the square-wave solution in the limit $\epsilon \rightarrow 0$.

Given γ_2 , we proceed to find a particular solution to Eq. (37). It turns out that the equations as written in the form given in (37) and (38) are not exactly solvable. Hence, since the equations are linear, we separate each equation into two parts, one of which is solvable analytically, while the other is solved numerically, i.e.

$$u_1(s) = u_{1c}(s) + u_{1-}(s); \quad v_1(s) = u_{1c}(s) + u_{1+}(s) \quad (45)$$

where the common function u_{1c} satisfies the equation

$$u_{1c}'' + 8(1 - 3u_0^2)u_{1c} = -2(4/3 + \gamma_2)u_0' + 8u_0^2u_0' \quad (46)$$

and $u_{1\pm}$ satisfies:

$$u_{1\pm}'' + 8u_{1\pm} - 24u_0^2u_{1\pm} = \pm 4\eta^2 \quad (47)$$

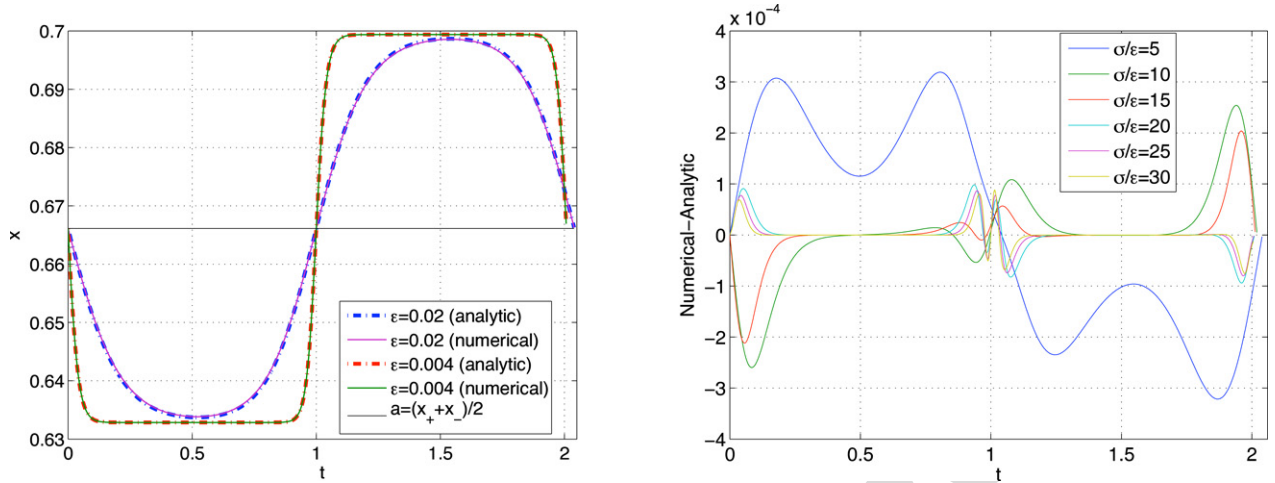


Fig. 3. Left: Closely matched, analytic and numerical waveforms for different values of ϵ at $\sigma = 0.1$. Right: The difference between the analytic solution and the numerical solution over a whole period for six different values of ϵ at $\sigma = 0.1$. The maximum error is $O(\sigma^3)$.

$u_{1\pm}$ can be obtained analytically and are given by:

$$u_{1\pm}(s) = \pm \left(\sqrt{1 - \eta^2} \right) \left(\frac{dn^2(z) + k^2 cn^2(z)}{4k} - \frac{cn(z)dn(z)}{2} \right). \quad (48)$$

u_{1c} is solved numerically using a spectral code and added to $u_{1\pm}$ to calculate u_1 and v_1 . The numerical algorithm for the spectral code is outlined in Appendix C.

3.3. Comparison of analytic results with numerical ones

Thus the analytic form of a SOPS can be written as

$$x(t) = a \pm b \left(u_0(t) + \sigma [u_{1c}(t) + u_{1\pm}(t)] + O(\sigma^2) \right) \quad (49)$$

where,

$$u_0(t) = \sqrt{1 - \eta} \operatorname{sn} \left(\frac{2\sigma}{\epsilon T} (\sqrt{1 + \eta})t, k \right); \quad k^2 = \frac{1 - \eta}{1 + \eta} \quad (50)$$

$$u_{1\pm}(t) = \pm \left(\sqrt{1 - \eta^2} \right) \left(\frac{dn^2(z, k) + k^2 cn^2(z, k)}{4k} - \frac{cn(z, k)dn(z, k)}{2} \right) \quad (51)$$

with $z = (2\sigma\sqrt{1 + \eta}t)/(\epsilon T)$. $u_{1c}(t)$ is obtained numerically by solving the equation:

$$u_{1c}''(s) + 8(1 - 3u_0^2(s))u_{1c}(s) = -2(4/3 + \gamma_2)u_0'(s) + 8u_0^2(s)u_0'(s); \quad (52)$$

with $s = (\sigma t)/(\epsilon T)$. Finally the period of each of $u_0(t)$, $u_{1c}(t)$ and $u_{1\pm}(t)$ and hence of $x(t)$ is given by

$$T = 2 + \epsilon(2 + c_{12}\sigma^2 + O(\sigma^3)); \quad c_{12} = -\frac{8}{15} - \frac{12}{5}\eta^2 \frac{(K(k) - E(k))}{(E(k) - \eta K(k))}. \quad (53)$$

We integrated the original delay equation (6), using the spectral algorithm outlined in Appendix B, and then compared the resulting SOPS over a period with the corresponding semi-analytic expression given above, by calculating the elliptic functions in MATLAB. The left side of Fig. 3 plots the numerical solution and the expression (49) over a single period in the two limits when the solution is sinusoidal and square-wave. The right side of Fig. 3 shows the difference between the two solutions on equally spaced points over a period. The maximum difference is $O(\sigma^3)$ as expected, since b in (49) above is $O(\sigma)$. Table 1 shows the maximum difference between the solutions over a period for four values of λ , close to the bifurcation value of the map and six values of ϵ spanning the entire space for which the solution is known to exist. The difference is $O(\sigma^3)$ as expected.

Thus for a given σ and ϵ , η can be calculated, using (34) which in turn gives k , the modulus of the elliptic functions, and hence an approximate solution to the original delay equation (6). In fact, the value of η depends on the ratio of σ to ϵ and it is this ratio that determines the shape of the solution and, in particular when the solution looks like a square-wave, the shape and the thickness of the transition layers connecting the plateaus in the solution. Fig. 4 plots $u_0(t)$ and $\sigma u_1(t) = \sigma(u_{1c}(t) + u_{1-}(t))$ and $\sigma v_1(t) = \sigma(u_{1c}(t) + u_{1+}(t))$ for a particular choice of parameters (λ , ϵ). It is clear that the amplitude of the approximate solution is determined by $u_0(t)$, while addition of $\sigma u_1(t)$ and $\sigma v_1(t)$ primarily contributes to the observed inequality in the half-periods of the solution by shifting the zero of $u_0(t)$ away from $T/2$.

Now the amplitude of $x(t)$, as given in (49) is thus, $b\sqrt{1 - \eta}$. Thus, for a given σ , in the limit $\epsilon \rightarrow 0$, $\eta \sim \exp(-\sigma/\epsilon) \rightarrow 0$ and the amplitude of $x(t)$ differs from b – the amplitude of the period-2 solution of the map – by an exponentially small term. As ϵ is increased, η increases and the amplitude of the solution begins to drop. In the other limit, as $\epsilon \rightarrow \epsilon_0(\sigma)$, the Hopf bifurcation value for a given σ , $\eta \rightarrow 1$ and the amplitude of the solution $\rightarrow 0$. This is expected, since according to the linear theory, these slowly oscillating periodic solutions do not exist if ϵ increases beyond $\epsilon_0(\sigma)$.

Table 1
Maximum difference over a whole period, between the numerical solutions and the analytic expressions for different values of σ and ϵ

$\sigma = 0.05$		$\sigma = 0.1$		$\sigma = 0.15$		$\sigma = 0.2$	
ϵ	Max. diff.	ϵ	Max. diff.	ϵ	Max. diff.	ϵ	Max. diff.
0.01	8.98E–05	0.02	3.22E–04	0.03	7.66E–04	0.04	2.01E–03
0.005	3.92E–05	0.01	2.60E–04	0.015	7.09E–04	0.02	1.47E–03
0.0034	2.68E–05	0.0067	2.12E–04	0.01	6.04E–04	0.013	1.29E–03
0.0025	3.26E–05	0.005	9.84E–05	0.0075	3.03E–04	0.01	8.11E–04
0.002	1.71E–05	0.004	8.68E–05	0.006	3.22E–04	0.008	1.14E–03
0.0017	2.91E–05	0.0034	8.82E–05	0.005	3.41E–04	0.0067	8.69E–04

The difference, as expected, is $O(\sigma^3)$.

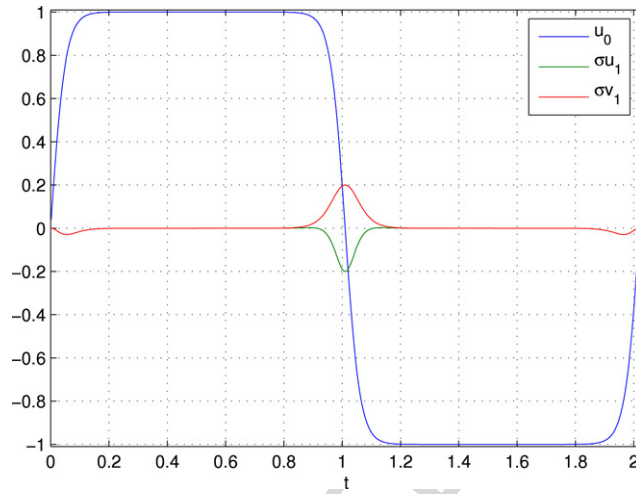


Fig. 4. Figure shows that the amplitude of $u_0(t)$ is not affected by the addition of $u_1(t)$ and $v_1(t)$, however the location of its zero at the half-period is changed. Here $\sigma = 0.2$ and $\epsilon = 0.01$.

4. Odd harmonic solutions

In the period-2 regime of the continuous logistic map given by,

$$x(t) = \lambda x(t-1)(1-x(t-1)) \quad (54)$$

there exist solutions other than the fundamental period-2 solution given by $x(t) = x_+$ for $t \in I^{2m}$ and $x(t) = x_-$ for $t \in I^{2m+1}$, where $I^m = (m, m+1]$. These other solutions, called the fissured solutions of n th degree (n :odd) by Ikeda et al. [20], are given by $x(t) = x_{\pm}$ for $t \in I_{2k}^{2m}$ and $x(t) = x_{\mp}$ for $t \in I_{2k-1}^{2m}$, where $I_k^m = (m+t_{k-1}, m+t_k]$, for $1 \leq k \leq (n+1)/2$, is the k th of the n subsections of I^m : $I_1^m = (m, m+t_1]$, $I_2^m = (m+t_1, m+t_2]$, ..., $I_n^m = (m+t_{n-1}, m+1]$ for an arbitrary sequence $\{t_k\}$ of t satisfying $0 < t_1 < t_2 < \dots < t_{n-1} < 1$. Clearly, there are infinitely many fissured solutions of a given degree. In the case of the delay equation (6) though, only a finite number of other solutions, which are the odd harmonics of the SOPS, can exist for a given value of ϵ and λ . In this section, we derive analytic expressions for these odd harmonics of (6) and then show that they are not stable against small perturbations, in the neighborhood of the first period-doubling bifurcation point of the map.

The existence of these odd harmonic solutions of Eq. (2) can be seen very easily [17,21,16,18], by transforming Eq. (2) to

$$\dot{x}(t) = -x(t) + f(x(t-r), \lambda) \quad (55)$$

where $r = 1/\epsilon$ is the value of the delay. Let us assume, that for a particular set of values of λ and r , there exists a SOPS, denoted by $x_r(t)$, whose period is given by $T(r) = 2r + c(\lambda)$, according to (53). Here c is a constant which depends only on λ as the period depends only linearly on $\epsilon = 1/r$. In this case, one can write, for some integer n ,

$$\dot{x}_r(t) = -x_r(t) + f(x_r(t-r-nT(r)), \lambda) \quad (56)$$

$$\dot{x}_r(t) = -x_r(t) + f(x_r(t-r_n), \lambda) \quad (57)$$

which implies that $x_r(t)$ is a solution of (55) for a higher value of delay $r_n = r + nT(r)$. However, clearly, $x_r(t)$ is not the SOPS of (57) as the SOPS, $x_{r_n}(t)$, of (57) has the period

$$T(r_n) = 2r_n + c(\lambda) = (2n+1)T(r). \quad (58)$$

This means, that $x_r(t)$ is the $(2n+1)$ th harmonic solution of (57), whose period is exactly $1/(2n+1)$ times the period of the SOPS of (57). Thus for a given value of λ , a SOPS of the delay equation (55) at a particular value of the delay $r(\epsilon)$ is an odd harmonic solution of order $(2n+1)$ of the equation with a higher (lower) value of delay $r_n(\epsilon_n)$. Conversely, for a given set of values of λ and ϵ , several odd-harmonic solutions can co-exist with the SOPS, if ϵ is sufficiently smaller than $\epsilon_0(\lambda)$, the value at which the SOPS is born. Clearly, there is a maximum number of these odd-harmonic solutions that can co-exist at these values of λ and ϵ , because an odd harmonic solution of order $(2n+1)$ for this set (λ, ϵ) is a SOPS of (λ, ϵ_n) , where ϵ_n must be smaller than $\epsilon_0(\lambda)$ for it to exist.

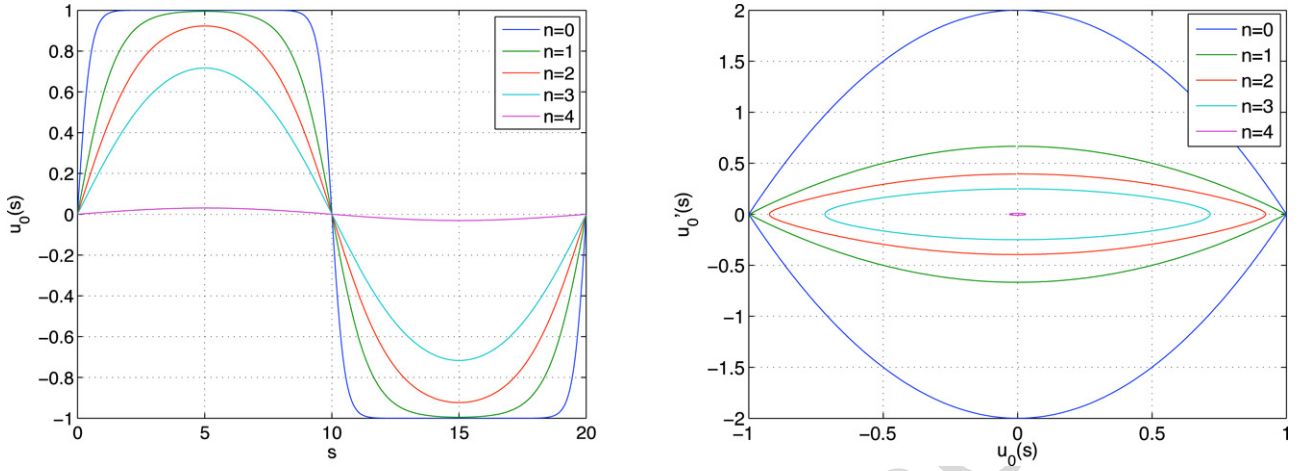


Fig. 5. Left: The first five odd harmonic solutions to Eq. (62) over a whole period in units of s ; their periods in units of t are different. Right: The phase space plot; the ninth harmonic is barely born. Here, $\sigma/\epsilon = 20$.

Thus while in the case of the map, all odd-harmonics of the period 2 solution exist in the entire period-2 regime of the map, only a finite number of them can co-exist in the case of the differential equation, and for a given value of λ , the upper bound on the number of possible odd-harmonic solutions depends on the value of the delay (ϵ).

We now derive a leading order analytic expression for these odd harmonic solutions, by solving the corresponding transition layer equations near the first period-doubling bifurcation point of the logistic map [3]. To begin with, a $(2n + 1)$ th harmonic solution to (6) is assumed to have a period $[2/(2n + 1)] + \delta_1 + \delta_2$; $n = 0, 1, 2, \dots$. The $n = 0$ case corresponds to the SOPS whose functional forms are derived in the last section. We now assume,

$$U(t) = x(t); \quad V(t) = x\left(t - \frac{1}{2n+1} - \delta_1\right). \quad (59)$$

Substituting in (6) and using the periodicity of the waveform gives,

$$\epsilon U'(t) + U(t) = f(\lambda, V(t + (n+1)\delta_1 + n\delta_2)); \quad n = 0, 1, 2, \dots \quad (60)$$

$$\epsilon V'(t) + V(t) = f(\lambda, U(t + (n+1)\delta_2 + n\delta_1)); \quad n = 0, 1, 2, \dots \quad (61)$$

The same expansions, in terms of (σ, ϵ) are assumed for δ_1 and δ_2 . Again changing the variable to $s = \sigma t/(\epsilon T)$ and assuming the same expansions for $u(s)$ and $v(s)$ in terms of σ , gives similar equations for u_0, u_1 and v_1 , albeit with different coefficients. Thus,

$$u_0'' + 2c_{10}^2(u_0 - u_0^3) = 0; \quad c_{10}(n) = \frac{2}{2n+1}; \quad n = 0, 1, 2, 3, \dots \quad (62)$$

$$u_1'' + 2c_{10}^2(1 - 3u_0^2)u_1 = -2(2c_{10}/3 + \gamma_2)u_0' + 4c_{10}u_0^2u_0' - c_{10}^2\eta^2 \quad (63)$$

$$v_1'' + 2c_{10}^2(1 - 3u_0^2)v_1 = -2(2c_{10}/3 + \gamma_2)u_0' + 4c_{10}u_0^2u_0' + c_{10}^2\eta^2. \quad (64)$$

Thus $u_0(t)$ is given by:

$$u_0(t) = \sqrt{1-\eta} \operatorname{sn}\left(\frac{2}{2n+1}(\sqrt{1+\eta})\frac{\sigma}{\epsilon T}t, k\right); \quad k^2 = \frac{1-\eta}{1+\eta}. \quad (65)$$

The expression for the period is given by:

$$T = \frac{2}{2n+1} + \epsilon \left(\frac{2}{2n+1} + c_{12}\sigma^2 + O(\sigma^3) \right) \quad (66)$$

$$c_{12} = -\frac{8}{15(2n+1)} - \frac{12}{5(2n+1)}\eta^2 \frac{(K(k) - E(k))}{(E(k) - \eta K(k))} \quad (67)$$

and η can be calculated by solving:

$$\frac{1}{2(2n+1)}\sqrt{1+\eta}\frac{\sigma}{\epsilon} = K(k); \quad k^2 = \frac{1-\eta}{1+\eta}. \quad (67)$$

It is evident that the value of η for the SOPS ($n = 0$), is equal to its value for the third harmonic ($n = 1$) solution if the ratio of σ to ϵ is thrice its value for the SOPS. Thus for a given σ and sufficiently small ϵ , several odd harmonic solutions can exist simultaneously.

Next, the functional form of $u_0(t)$ as given in (62) is used as an initial function to integrate the original delay equation, using the spectral method outlined in Appendix B. We observe that such an initial function is not attracted to the corresponding odd harmonic solution, but instead settles to the corresponding SOPS. This implies that the odd harmonic solutions are not stable against small perturbations in the neighborhood of the first period-doubling bifurcation point of the map.

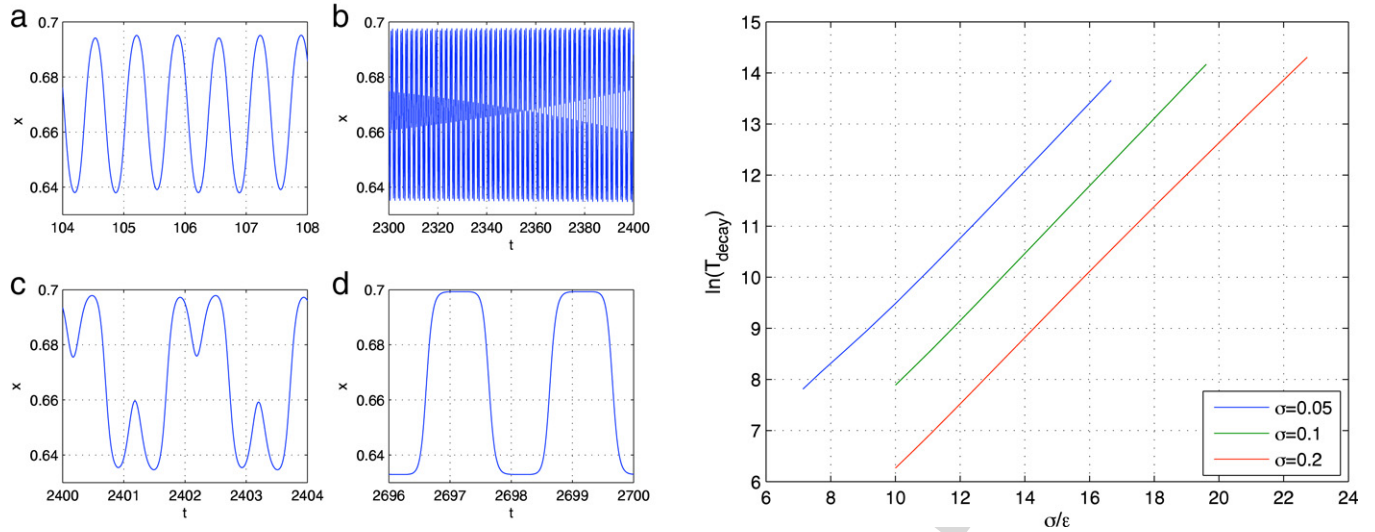


Fig. 6. Left: The decay of the leading order approximation to the third harmonic to the SOPS. Here $\sigma = 0.1$ and $\epsilon = 0.01$. Right: The logarithm of time of decay as a function of σ/ϵ . The linear plot and same slopes for different values of σ suggests that $T_{\text{decay}} \propto \exp \sigma/\epsilon$.

We measure the time of decay of these initial functions in terms of the number of intervals for which they survive, by measuring the number of zeroes of the derivative of the solution in a given interval. Fig. 6 shows the decay of an initial function consisting of 3 transition layers, expressed by the leading order approximation for the third harmonic solution, in a single initial time interval of length 1. The decay happens with two of the layers collapsing together. The right side of Fig. 6 plots log of the time of decay of the third harmonic as a function of σ/ϵ , for three different values of σ . The time of decay increases exponentially as a function of σ/ϵ , thus, for extremely small values of ϵ , these initial functions can be very long lived. Since the lines for different values of σ are almost parallel, one can write, $T_{\text{decay}} = c_1(\sigma) \exp(c_2 \sigma/\epsilon)$ where c_1 and c_2 are constants and c_1 is dependent of σ .

5. Conclusion

In this paper, we have derived approximate analytic expressions for slowly oscillating periodic solutions of a singularly perturbed delay differential equation with logistic nonlinearity. These expressions, derived using a two-parameter perturbation expansion in terms of ϵ , the ratio between the linear decay time (τ) of the dependent variable and the delay time, and σ , which depends on the distance from the period-doubling bifurcation point of the underlying map, and the scaling $\epsilon = O(\sigma^2)$, match accurately with the corresponding numerical solutions. We were also able to derive accurate expressions for the period of these solutions. In particular, the calculation of first order correction to the leading order expression, explains the observed asymmetry of square-wave solutions mentioned in the introduction. In the distinguished limit, $\epsilon = O(\sigma^2)$, these solutions resemble square-waves, however, as ϵ approaches $\epsilon_0 = O(\sigma)$, the Hopf bifurcation value, they become sinusoidal. We found a close agreement between the analytic expressions and the numerical forms for the sinusoidal solutions as well. Further, we were able to demonstrate the gradual change in the amplitude of these solutions as they change their shape from sinusoidal to square, using the analytic expressions derived.

Erneux et al. [10] employ a modified Poincaré–Lindstedt method to solve the original delay equation (2). By using the scaling $\sigma = \Lambda \epsilon$, they track the bifurcation curve uniformly, with the parameter Λ determining the character of the solutions from sinusoidal to square. However, in this treatment, the leading order equation changes if ϵ is of lesser order. By using the present scaling, $\epsilon = O(\sigma^2)$, we are able to give a unified treatment that remains qualitatively unchanged if ϵ is of any lesser order, including $\epsilon \rightarrow 0$ for σ fixed. In fact, the nonlinear ODE for u_0 remains unchanged for all such limit processes, allowing us to introduce η as an independent parameter, that can assume any value in the interval $[0, 1]$.

By using the same perturbative approach, we have also derived analytic expressions for odd harmonic solutions of the delay equation, near the first period-doubling bifurcation point of the underlying map. We have then shown that these odd harmonic solutions are not stable against small perturbations. That is, if one integrates Eq. (6), starting with a leading order approximation for an odd harmonic solution, then while such a form can remain extremely long-lived for a very small value of ϵ , the solution is driven away from the odd harmonic and eventually settles to the corresponding slowly oscillating periodic solution. While a logistic form of nonlinearity is taken as a prototype for this study, as shown in Appendix A, our treatment can be easily modified for a general form of nonlinearity such as the Ikeda model [17] and similar results can be obtained.

Numerical integration of the original delay equation was done using an accurate spectral algorithm [9,8]. The efficiency and accuracy of this scheme in obtaining stiff solutions of delay equations was checked by comparing it with the state-of-the-art time-stepping algorithm as outlined in Appendix B.

Uncited references

Appendix A. The case of a generic nonlinearity

The derivation for the analytic expressions for the SOPS to Eq. (6) can be modified easily to the case of Eq. (2) with a general nonlinearity:

$$\epsilon \dot{x}(t) = -x(t) + f(x(t-1), \lambda), \quad t \geq 0 \quad (\text{A.1})$$

where it is assumed that the map $f(x, \lambda)$ undergoes a period-doubling bifurcation at $\lambda = \lambda_0$ when $x_0 = f(x_0, \lambda_0)$, the fixed point of the map, becomes unstable. The transition layer equations remain the same as defined in Eqs. (18) and (19).

$$\epsilon U'(t) + U(t) = f(\lambda, V(t + \delta_1)) \quad (\text{A.2})$$

$$\epsilon V'(t) + V(t) = f(\lambda, U(t + \delta_2)) \quad (\text{A.3})$$

except the “half-periods”, $1 + \delta_1$ and $1 + \delta_2$ are defined as the time intervals between successive crossings of the solution with x_0 , the unstable fixed point of the map. Again, δ_1 and δ_2 are assumed to have similar expansions in terms of ϵ and $\sigma = \sqrt{\lambda - \lambda_0}$. Next $U(t)$ and $V(t)$ are expanded in powers of σ about x_0 :

$$U(t) = x_0 - [\sigma u_0(t) + \sigma^2 u_1(t) + O(\sigma^3)]$$

$$V(t) = x_0 + [\sigma v_0(t) + \sigma^2 v_1(t) + O(\sigma^3)].$$

Transforming to $s = \frac{\sigma t}{\epsilon}$, substituting the corresponding expansions in the transition layer equations and matching orders by using the scaling $\epsilon \sim O(\sigma^2)$ gives the following equation for $u_0(s) = v_0(s)$:

$$u_0''(s) + 4Au_0(s) - 4Bu_0^3(s) = 0 \quad (\text{A.4})$$

where,

$$A = -[f_{\lambda} f_{xx0} + 2f_{x\lambda 0}]; \quad B = \left[\frac{1}{2} f_{xx0}^2 + \frac{1}{3} f_{xxx0} \right]. \quad (\text{A.5})$$

Here, $f_{x0} = f_x(\lambda_0, x_0)$ and so on. Integral curves of (A.4) are given by:

$$\frac{1}{2} u_0'^2 + 2Au_0^2 - Bu_0^4 = C. \quad (\text{A.6})$$

Choosing $C = A^2(1 - \eta^2)/4B$ and following the arguments in Section 3, one finds that the solution is given by the Jacobi elliptic function:

$$u_0(s) = \sqrt{\frac{A}{B}(1 - \eta)} \operatorname{sn} \left(\sqrt{\frac{A}{2}(1 + \eta)} s, k \right) \quad (\text{A.7})$$

where, k is the modulus of the Jacobi elliptic functions. The equations for $u_1(s)$ and $v_1(s)$ are:

$$u_1'' + 4(A + 3u_0^2 B)u_1 = -2 \left(c_{20} + \frac{2A}{3} \right) u_0' - 4Bu_0^2 u_0' - D_1 \eta^2 - D_2 \frac{u_0'''}{u_0'} \quad (\text{A.8})$$

$$v_1'' + 4(A + 3u_0^2 B)v_1 = -2 \left(c_{20} + \frac{2A}{3} \right) u_0' - 4Bu_0^2 u_0' + D_1 \eta^2 + D_2 \frac{u_0'''}{u_0'}$$

where

$$D_1 = \frac{A^2 c_{10}^2}{4B} f_{xx0}; \quad D_2 = \frac{A f_{xx0} - 2B f_{\lambda 0}}{4B}. \quad (\text{A.8})$$

which again can be solved, partly numerically and partly analytically. Expression for the period of the solution turns out to be

$$T = 2 + \epsilon(2 + c_{12}\sigma^2 + O(\sigma^3)); \quad c_{12} = -\frac{2Ac_{10}}{15} - \frac{3Ac_{10}}{5} \eta^2 \frac{(K(k) - E(k))}{(E(k) - \eta K(k))}. \quad (\text{A.8})$$

Appendix B. Numerical method

The numerical algorithm used for integrating singularly perturbed delay equations of the type considered in this article is an efficient and accurate spectral method developed by Coutsias et al. [9,8] to integrate ordinary differential equations with rational function coefficients. This section sketches the algorithm first [3] and then compares its accuracy, in obtaining periodic solutions to linear delay equations and square wave SOPS to singularly perturbed delay equations, with that of RADAR5, a Runge–Kutta algorithm [12].

The method of Coutsias et al. [9,8] basically achieves efficient approximate inversion of linear differential operators with rational function coefficients. It employs an expansion in terms of a large class of orthogonal polynomial families, including all the classical orthogonal polynomials. These families obey a simple 3-term recurrence relation for differentiation, and hence the problem reduces to solving such recurrence relations efficiently. Gautschi's seminal paper on “Computational properties of three-term recurrence relations” [11] gives a comprehensive account of the use of such equations and describes the algorithm originally devised by J.C.P. Miller [1] for the computation of tables of the modified Bessel function for solving such recurrence relations. This algorithm, which uses the technique of backward recurrence is extremely accurate as shown by Olver [25].

The algorithm is very well suited for delay equations of the form:

$$a\dot{x}(t) + bx(t) = f(x(t-r), \lambda). \quad (\text{B.1})$$

When $x(t)$ is expanded in terms of a suitable orthogonal polynomial family over an interval of length r , the linear differential operator on the left hand side transforms to a tri-diagonal matrix operating on the mode-space coefficients of x . The right-hand side of the above equation, although nonlinear, is completely known as the solution for the previous interval of length r is assumed known. Thus in the mode-space, Eq. (B.1) reduces to an inhomogeneous three term difference equation, which can be solved. Having obtained the solution on an interval say $[rn, r(n+1)]$, the process can be repeated to obtain the solution on $[r(n+1), r(n+2)]$ by substituting the previously obtained solution in the right hand side of (B.1).

B.1. The algorithm

Here we sketch the key steps involved in this algorithm. We use the Chebyshev polynomials, $T_n(x)$, that are orthogonal on $[-1, 1]$ over the weight $(1-x^2)^{-1/2}$, for the expansions. Then solving the delay equation of the form (B.1), essentially reduces to solving the following ordinary differential equation

$$\dot{x}(t) + x(t) = f(t), \quad -1 \leq t \leq 1, \quad x(-1) = x_0. \quad (\text{B.2})$$

Expanding each term of above equation in terms of Chebyshev polynomials gives,

$$x(t) = \sum_{n=0}^N x_n^{(0)} T_n(t), \quad \dot{x}(t) = \sum_{n=0}^N x_n^{(1)} T_n(t), \quad f(t) = \sum_{n=0}^N f_n T_n(t).$$

N , the resolution or the point of truncation in the sum above is decided by the level of accuracy required, which in turn is decided by the stiffness of the equation one wishes to solve. The spectral method determines the expansion coefficients directly, from which the solution can be computed at any point t in the interval. Next we choose the Chebyshev grid for the points space, $t_m = \cos(m\pi/N)$, so that each expansion reduces to a cosine discrete Fourier transform, since $T_n(\cos(m\pi/N)) = \cos(n\pi m/N)$. Finally using a recurrence relation for the Chebyshev polynomials and the fact that they form a complete basis, one can obtain the following difference equation for the expansion coefficients $x_n^{(0)}$:

$$c_{n-1}x_{n-1}^{(0)} + 2anx_n^{(0)} - x_{n+1}^{(0)} = c_{n-1}f_{n-1} - f_{n+1}; \quad n = 1, 2, \dots, N \quad (\text{B.3})$$

where, $c_0 = 2, c_n = 1$ for $n = 1, 2, \dots, N$ and $f_{N+1} = x_{N+1}^{(0)} = 0$. The homogeneous part of Eq. (B.3) is precisely the three-term recurrence relation obeyed by Bessel functions.

The solution to Eq. (B.3) can be written in terms of a homogeneous solution and a particular solution. The homogeneous solution is a linear combination of a minimal solution and a dominant solution denoted by y_n and Y_n respectively. They can be obtained by defining the ratios, $r_n = \frac{y_{n+1}}{y_n} \rightarrow 0$ and $R_n = \frac{Y_{n+1}}{Y_n} \rightarrow \infty$ as $n \rightarrow \infty$ and solving for them by writing the homogeneous form of (B.3) in terms of them:

$$r_{n-1} = \frac{1}{2an + r_n}; \quad R_n = -2an + \frac{1}{R_{n-1}}. \quad (\text{B.4})$$

Thus r_n can be obtained using a backwards recursion, by assuming $r_\nu = 0$ for some $\nu > N$. By doing this, any error corresponding to triggering the dominant solution dies out quickly. Once all the ratios are found, the minimal solution can be obtained up to a normalising factor.

Since the dominant and the minimal solution should be linearly independent, the starting value R_0 for this forward recursion is determined by requiring that the vector (Y_0, Y_1) be orthogonal to (y_0, y_1) , which leads to $R_0 = -1/r_0$.

Next, the full solution to (B.3) can be written in the form,

$$x_n^{(0)} = z_n + Ay_n; \quad n = 0, 1, \dots, N. \quad (\text{B.5})$$

Here, $z_n = A_n y_n + B_n Y_n$ is the particular solution. Redundance in the determination of A_n and B_n allows one to rewrite Eq. (B.3) in terms of $u_n = A_n y_n$ and $v_n = B_n Y_n$ as [3],

$$u_n = u_{n-1}r_{n-1} - \tau_n; \quad v_n = v_{n-1}R_{n-1} + \tau_n; \quad \tau_n = \frac{f_n}{R_n - r_n} \quad (\text{B.6})$$

u_0 can be chosen arbitrarily and u_n could be determined. However, since its calculation involves R_n , v_n must be found in a numerically stable manner by solving the recursion relation backwards by setting $v_\nu = 0$, for the same ν as in the solution of y_n . Finally the constant A in (B.5) is found using the initial condition,

$$x_0 = \sum_{n=0}^N (-1)^n x_n^{(0)} \dots T_n(-1) = (-1)^n. \quad (\text{B.7})$$

Upon obtaining $\hat{x}^{(0)}$, the solution $x(t_n)$ is obtained by taking the inverse Fourier transform.

B.2. A comparison

Currently the numerical schemes used most often to integrate delay-differential equations involve standard time-stepping methods with adaptive stepsize control. This section compares the accuracy of the spectral method with that of RADAR5, a fifth order Runge-Kutta method with adaptive step-size control [12,4], to integrate (a) linear delay equations, whose exact solutions are known and (b) stiff delay differential equations such as the singularly perturbed delay differential equation considered in this article.

Table B.1

The difference (Δ_1 and Δ_2) between the numerical solutions (using the spectral method) and analytic solutions to Eqs. (B.9) and (B.10) respectively, after over a million iterations

Resolution	Error in the numerical solution	
	Δ_1	Δ_2
8	0.626 E–06	0.261 E–04
16	0.486 E–10	0.213 E–08
⋮	⋮	⋮
1024	0.490 E–10	0.212 E–08

Table B.2

The difference between the analytical solution and the numerical solution obtained using RADAR5, to Eqs. (B.9) and (B.10) for several tolerances

Relative tolerance	Maximum step-size	Cumulative error in x_1 ($t = 10^6$)	Maximum step-size	Cumulative error in x_2 ($t = 10^6$)
1.0 E–07	0.01	0.911 E–04	0.1	0.160 E–02
1.0 E–09	0.1	0.667 E–04	0.1	0.126 E–03
1.0 E–11	0.1	0.110 E–04	0.1	0.448 E–05
1.0 E–13	0.1	0.084 E–04	0.1	0.552 E–05

B.2.1. Linear delay equations

We consider the linear delay equations of the following form:

$$\dot{x}(t) + \alpha x(t) + \beta x(t - r) = 0; \quad t \geq 0. \quad (\text{B.8})$$

The following two choices of parameter values yield stable periodic solutions to this equation, such that the corresponding characteristic equation has exactly two purely imaginary roots while the other roots have negative real parts.

- $\alpha = -1$, $\beta = \sqrt{2}$ and $r = \pi/4$. The general solution is a linear combination of $\sin(t)$ and $\cos(t)$. Specifically we solve the following equation with $\sin(t)$ as a solution using both numerical schemes.

$$\frac{dx_1}{dt} = x_1(t) - \sqrt{2}x_1\left(t - \frac{\pi}{4}\right); \quad t \geq 0 \quad (\text{B.9})$$

with, $x_1(t) = \sin(t)$; $t \in [-\pi/4, 0]$.

- In the previous example, the period of the solution is 2π which is commensurate with the delay. This restriction is taken out in this example by choosing $\alpha = -1$, $\beta = \sqrt{3}$ and $r = \frac{\tan^{-1}(\sqrt{2})}{\sqrt{2}}$. The general solution in this case is a linear combination of $\sin(\sqrt{2}t)$ and $\cos(\sqrt{2}t)$ and in particular $\sin(\sqrt{2}t)$ is chosen for the computation.

$$\frac{dx_2}{dt} = x_2(t) - \sqrt{3}x_2(t - r); \quad t \geq 0; \quad r = \frac{\tan^{-1}(\sqrt{2})}{\sqrt{2}} \quad (\text{B.10})$$

with $x_2(t) = \sin(\sqrt{2}t)$; $t \in [-r, 0]$.

Table B.1 shows the error in the numerical solution of Eq. (B.8) at $t = 10^6$, obtained using the spectral scheme outlined above. Note that the integration is done in steps of the delay which is less than 1, hence the number of times the equation is integrated is over a million.

Table B.2 gives the errors in the numerical solutions (x_1, x_2) of Eq. (B.8) for the two sets of parameters mentioned above, obtained using RADAR5 for different values of the relative tolerance. The maximum allowed step-size mentioned below is the optimal value for each tolerance, that balances the size of the error and the total number of function calculations.

B.2.2. Singularly perturbed delay differential equation

Now we take the following singularly perturbed delay differential equation considered in this article

$$\epsilon \dot{x}(t) = -x(t) + \lambda x(t - 1)(1 - x(t - 1)) \quad (\text{B.11})$$

and integrate it, using both the spectral method and RADAR5 for a million intervals. An asymptotic form of a slowly oscillating periodic solution over a single interval, obtained after integrating (B.11) over 10 000 intervals using the spectral method, is used as the initial function for both methods. Then, for each method, we calculate the phase error, $\Delta\Phi$, defined as:

$$\Delta\Phi_n = |t_n - t'_n|; \quad n = 1, 101, 201, \dots \quad (\text{B.12})$$

where t_n are the values of every hundredth time instances at which the numerical solutions cross x_0 , the unstable fixed point of the map, and $t'_n = t_1 + (n - 1)T/2$, with T being the asymptotic expression for the period of the solution given in (44):

$$T \approx 2 + 2\epsilon \left(1 - \frac{4}{15}\sigma^2 + O(\sigma^3)\right). \quad (\text{B.13})$$

The slowly oscillating periodic solution of Eq. (B.11) becomes square-wave like when $\epsilon = O(\sigma^2)$ or smaller. Hence the transition layers in the solution become sharper and hence the solution becomes stiffer as ϵ decreases. Since the asymptotic expression for the period is known only up to $O(\sigma^2)$, an inherent, minimum phase error of $O(\epsilon\sigma^3)$ is introduced over each cycle in these computations.

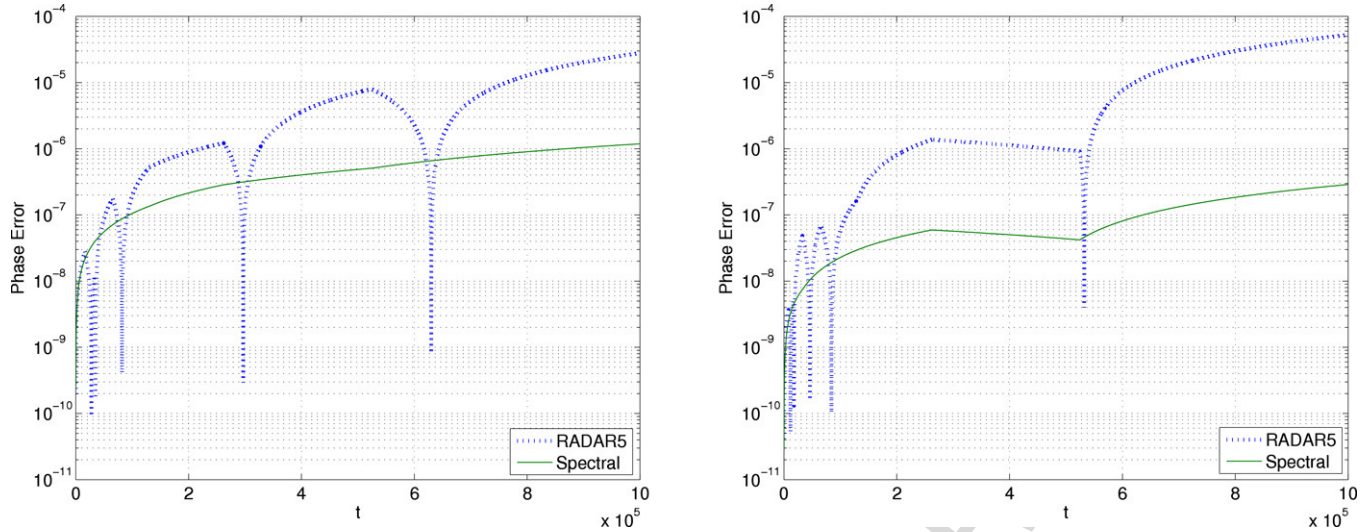


Fig. B.1. Plot of the phase error in the integration of Eq. (B.11) by RADAR5 and the spectral method. Here $\sigma = 0.01$ and $\epsilon = 5.0E-4$ for the left figure and $\epsilon = 1.0E-4$ for the right one. The solid red curve, $\epsilon\sigma^4 t$, is shown for comparison. The spectral method tracks the phase almost exactly; the error is of the same order as the error in the analytical formula itself.

Fig. B.1 shows the comparison plots of the phase error obtained by the spectral method and RADAR5 for $\epsilon = 5.0E-4$ and $1.0E-4$ with $\sigma = 0.01$. The resolution for the spectral method, in both cases was 8192. A maximum stepsize of $1.0E-4$ was set for RADAR5 and a dense output obtained at an interval of size $1.0E-5$ was used to find the values of t_n . As the figure shows, the spectral method tracks the phase of the SOPS almost exactly, hence, the error is of the same order as the error in the analytical formula itself. The phase error calculated by RADAR5 fluctuates and the difference between t_n and t'_n changes sign which causes the spikes observed in the figure. Hence, it is the maxima that give an estimate of the error bar associated with that calculation.

Appendix C. Numerical algorithm to calculate u_{1c}

Here, we give the numerical algorithm we use to calculate u_{1c} by integrating equation (47) which is of the form:

$$y''(t) + f(t)y(t) = g(t) \quad (C.1)$$

where $f(s)$ and $g(s)$ are periodic functions of t of known period T . We solve this equation on $[0, T)$ in MATLAB using the following steps:

- Since the differential operator in this case consists of periodic coefficients, we use Fourier transform on a equally spaced grid over the period T :

$$f(t_l) = \frac{1}{N} \sum_{m=-N/2+1}^{N/2} \hat{f}_m e^{2\pi i l m / N}; \quad g(t_l) = \frac{1}{N} \sum_{m=-N/2+1}^{N/2} \hat{g}_m e^{2\pi i l m / N} \quad (C.2)$$

and,

$$y(t_l) = \frac{1}{N} \sum_{m=-N/2+1}^{N/2} \hat{y}_m e^{2\pi i l m / N}; \quad t_l = \frac{l}{N} T; \quad l = 0, 1, \dots, N-1. \quad (C.3)$$

- Multiplying $f(t)$ and $y(t)$ gives a convolution matrix, which is a $(2N-1) \times N$ matrix of Fourier coefficients of $f(t)$ and acts on a column vector of \hat{y}_m s of length N . Further, in the mode space $y''(t)$ can be represented as a $(N \times N)$ diagonal matrix \hat{D} and $g(t)$ is represented by a column vector of \hat{g}_m s of length N . We crop the convolution matrix so as to form a $(N \times N)$ toeplitz matrix \hat{C} to write the equation:

$$\left[\frac{-4\pi^2}{T^2} \hat{D} + \hat{C} \right] \hat{Y} = \hat{G}. \quad (C.4)$$

Here, the coefficients in the column vector \hat{Y} and \hat{G} are re-ordered to be consistent with \hat{C} .

- Next, we use the initial condition $y(0) = a$:

$$\frac{1}{N} \sum_{m=-N/2+1}^{N/2} \hat{y}_m = a. \quad (C.5)$$

Thus we add a row of ones to the square matrix on the left hand side of Eq. (C.4), and add the entry a to the column on the right hand side.

- Finally, we solve the resulting matrix equation of the form $AX = B$ where A is $((N+1) \times N)$ and B is a column vector with N components, by using the "mldivide" function or the "\" operator in MATLAB. $X = A \setminus B$ is the solution in the least square sense to the under- or overdetermined system of equations $AX = B$. In other words, X minimizes the $norm(A * X - B)$, the length of the vector $AX - B$.

References

- [1] Bessel Functions, Part II, in: *Mathematical Tables*, vol. v.X, Cambridge University Press, 1952.
- [2] M. Abramowitz, I.A. Stegun, *Handbook of Mathematical Functions with Formulas, Graphs, and Mathematical Tables*, National Bureau of Standards, Washington D.C., 1981.
- [3] M.H. Adhikari, Numerical and asymptotic studies of delay-differential equations, Doctoral dissertation, University of New Mexico, Albuquerque, NM, USA, Dec 2007.
- [4] A. Bellen, M. Zennaro, *Numerical Methods for Delay Differential Equations*, Springer-Verlag, New York, 2003.
- [5] P. Byrd, M. Friedman, *Handbook of Elliptic Integrals for Engineers and Physicists*, Springer, Berlin, 1954.
- [6] S.N. Chow, J.K. Hale, W. Huang, From sine waves to square waves in delay equations, *Proc. Roy. Soc. Edinburgh Sect. A-Math.* 120 (1992) 223–229.
- [7] S.N. Chow, J. Mallet-Paret, Singularly perturbed delay differential equations, in: *Coupled Nonlinear Oscillators*, in: *Proceedings of the Joint U.S. Army - Center for Nonlinear Studies Workshop*, Los Alamos, New Mexico, 1983, pp. 7–12.
- [8] E.A. Coutsias, T. Hagstrom, J. Hesthaven, D. Torres, Integration preconditioners for differential operators in spectral τ -methods, in: Andrew V. Ilin, L. Ridgway Scott (Eds.), *Proceedings of ICOSAHOM 3*, *Houston Journal of Mathematics* (1996), 21–38 (special issue).
- [9] E.A. Coutsias, T. Hagstrom, D. Torres, An efficient spectral method for ordinary differential equations with rational function coefficients, *Math. Comput.* 65 (214) (1996) 611–635.
- [10] T. Erneux, L. Larger, M.W. Lee, J.P. Goedgebuer, Ikeda hopf bifurcation revisited, *Physica D* 194 (1–2) (2004) 49–64.
- [11] W. Gautschi, Computational aspects of three-term recurrence relations, *SIAM Rev.* 9 (1) (1967) 24–82.
- [12] N. Guglielmi, E. Hairer, Implementing radau iia methods for stiff delay differential equations, *Computing* 67 (1) (2001) 1–12.
- [13] J.K. Hale, W.Z. Huang, Period-doubling in singularly perturbed delay equations, *J. Differential Equations* 114 (1) (1994) 1–23.
- [14] J.K. Hale, W.Z. Huang, Periodic solutions of singularly perturbed delay equations, *Z. Angew. Math. Phys.* 47 (1) (1996) 57–88.
- [15] K. Ikeda, Multiple-valued stationary state and its instability of the transmitted light by a ring cavity system, *Opt. Commun.* 30 (2) (1979) 257–261.
- [16] K. Ikeda, Chaos and optical bistability: Bifurcation structure, in: L. Mandel, E. Wolf (Eds.), in: *Coherence and Quantum Optics*, vol. V, 1984, pp. 875–882.
- [17] K. Ikeda, O. Akimoto, Successive bifurcations and dynamical multi-stability in a bistable optical-system – a detailed study of the transition to chaos, *Appl. Phys. B* 28 (2–3) (1982) 170–171.
- [18] K. Ikeda, O. Akimoto, Optical turbulence, in: Y. Kuramoto (Ed.), *Chaos and Statistical Methods: Proceedings of the Sixth Kyoto Summer Institute*, Kyoto, Japan, 1983, pp. 249–257.
- [19] K. Ikeda, H. Daido, O. Akimoto, Optical turbulence - chaotic behavior of transmitted light from a ring cavity, *Phys. Rev. Lett.* 45 (9) (1980) 709–712.
- [20] K. Ikeda, K. Kondo, O. Akimoto, Successive higher-harmonic bifurcations in systems with delayed feedback, *Phys. Rev. Lett.* 49 (20) (1982) 1467–1470.
- [21] K. Ikeda, K. Matsumoto, High-dimensional chaotic behavior in systems with time-delayed feedback, *Physica D* 29 (1–2) (1987) 223–235.
- [22] M.C. Mackey, L. Glass, Oscillation and chaos in physiological control-systems, *Science* 197 (4300) (1977) 287–288.
- [23] J. Mallet-Paret, R. Nussbaum, A bifurcation gap for a singularly perturbed delay equation, in: M.F. Barnsley, S.G. Demko (Eds.), *Chaotic Dynamics and Fractals*, 1986, pp. 263–286.
- [24] J. Mallet-Paret, R.D. Nussbaum, Global continuation and asymptotic behavior for periodic solutions of a differential-delay equation, *Ann. Mat. Pura Appl.* 145 (1986) 33–128.
- [25] F. Olver, Error analysis of miller's recurrence algorithm, *Math. Comput.* 18 (85) (1964) 65–74.
- [26] M.R. Semak, Asymptotic and numerical studies of a differential-delay system, Doctoral dissertation, University of New Mexico, Albuquerque, NM, USA, Jul 2000.